

## Phase space structure of spinning disks

Mir Abbas Jalali\*, Arzhang Angoshtari

*Department of Mechanical Engineering, Center of Excellence in Design, Robotics and Automation, Sharif University of Technology,  
P.O. Box: 11365-9567, Azadi Avenue, Tehran, Iran*

Received 10 April 2006; accepted 10 April 2006

### Abstract

Using a Hamiltonian formalism and a sequence of canonical transformations, we show that the ordinary differential equations associated with the forced oscillations of rotating circular disks admit the first integral of motion. This reduces the phase space dimension of the governing equations from five to three. The phase space flows of the reduced system are then visualized using Poincaré maps. Our results show that single mode oscillations of rotating disks are subject to chaotic behavior through the emergence of higher-order resonant islands that surround fundamental periodic cycles. We extend our new formalism to imperfect disks and construct adiabatic invariants near to and far from resonances. For low-speed imperfect disks, we find a new kind of bifurcations of the phase space flows as the system parameters vary. We study the effect of structural damping using Hamilton's principle for non-conservative systems and reveal the existence of asymptotically stable limit cycles for the damped system near the 1:1 resonance. We show that a low-speed disk is eventually flattened due to damping effect.

© 2006 Elsevier Ltd. All rights reserved.

*Keywords:* Spinning disks; Chaos; Non-linear dynamical systems; Canonical transformations; Resonances; Adiabatic invariants; Limit cycles

### 1. Introduction

Thin spinning disks are important components of hard disk drives (HDDs), optical drives and circular saws. Lateral oscillations induced by external forces, internal resonances and initial imperfections are hazardous in these applications. Identification of optimum operating conditions of spinning disks is a critical step in their design and fabrication processes. For example, while data access rate of a HDD is improved by increasing the angular velocity  $\Omega_0$  of the disk, the head-induced lateral vibration of the disk continuously changes the air gap between the disk and the head. This effect may cause disk crash if the air gap is closed.

In his pioneering work, Nowinski [1] derived the governing equations of the transverse, non-linear oscillations of spinning circular disks. Almost four decades later, approximate solutions of his equations were found by Raman and Mote [2,3]. They used eigenfunctions of the associated linear problem and reduced the governing non-linear partial differential equations

(PDEs) to a set of ordinary differential equations (ODEs) using Galerkin's projection technique [4]. They attempted to solve the resulting ODEs through a first-order averaging method and studied bifurcations and stability of the averaged equations. Luo and Tan [5] adopted a similar method for a more complete model of the governing PDEs. Their model included the effects of rotation-induced Coriolis and centrifugal forces, but they ignored lateral forces that result in time-dependent Hamiltonians. Finite difference and finite element methods have also been used by some authors [6,7] for vibration analysis of spinning disks.

Works in the literature and those quoted above contain valuable results for the spinning disk problem, but they are still incapable of providing a global picture of phase space flows. Specifically, prediction of chaotic behavior has remained as an open problem. This paper deals with the equations of motion for the amplitude functions of a single radial and azimuthal mode of a spinning disk subject to the periodic action of a lateral, point force. We present our new Hamiltonian formalism in Section 2 using Deprit's [8] Lissajous variables. We introduce two successive canonical transformations which remove time from the resulting Hamiltonian and we find a new first integral. We generate the Poincaré maps of the motion equations

\* Corresponding author. Tel.: +98 21 6616 5688.

*E-mail addresses:* [mjalali@sharif.edu](mailto:mjalali@sharif.edu) (M.A. Jalali),  
[arzhang\\_a@mehr.sharif.edu](mailto:arzhang_a@mehr.sharif.edu) (A. Angoshtari)

*URL:* <http://sina.sharif.edu/~mjalali> (M.A. Jalali).

(expressed in the action-angle variables) in Section 3 and unveil the global geometry of phase space flows. We investigate the effect of imperfections in Section 4 and construct adiabatic invariants for high- and low-speed disks and also near the 1:1 resonance. We analytically investigate the effect of damping in Section 5. We summarize our results in Section 6 and discuss on possible ways of controlling lateral vibrations by introducing optimum operation conditions. Approximations of Nowinski’s [1] theory are also explained in Section 6.

## 2. Hamiltonian formalism and the first integral

Denote  $(R, \phi)$  as the usual polar coordinates and consider the lateral displacement field

$$w(R, \phi, t) = U(R)[x(t) \cos n\phi + y(t) \sin n\phi], \quad (1)$$

for a spinning circular disk with the angular velocity  $\Omega_0$ .  $U(R)$  is a single radial eigenfunction and  $n$  is the azimuthal wave number. Raman and Mote [2] assumed the point force  $(f_l/R)\delta(R - R_0)\delta(\phi - \Omega_0 t)$  and applied Galerkin’s method [4] to derive the following differential equations of motion for the amplitude functions  $x(t)$  and  $y(t)$ :

$$\ddot{x} + \omega^2 x + \gamma(x^2 + y^2)x = F \cos(n\Omega_0 t), \quad (2a)$$

$$\ddot{y} + \omega^2 y + \gamma(x^2 + y^2)y = F \sin(n\Omega_0 t), \quad (2b)$$

where  $\omega, \gamma > 0$  and  $F$  are constant coefficients and we have

$$F = \frac{f_l U(R_0)}{\pi \int [U(R)]^2 dR}. \quad (3)$$

For instance, in a HDD,  $f_l$  is the aerodynamic lift generated between the head and the disk, and  $R_0$  is its fixed radial location which is associated with a track. Eq. (3) shows the major role of  $R_0$  in determining the amplitude of forcing terms. Classical compressible Navier–Stokes equations cannot be used for modeling the air flow inside the gap because the Knudsen number  $K_n = \lambda/\Delta$  is of  $\mathcal{O}(1)$  in a typical HDD. Here  $\lambda$  is the mean free path of the air molecules and  $\Delta$  is the size of the gap. For  $\Delta = 70$  nm and  $\lambda = 10$  nm we get  $K_n \approx 0.14$  which is marginal. Hence, one needs to use Boltzmann equation and molecular dynamics techniques to compute  $f_l$ . This is the subject of ongoing research in computer industry. In general, we may assume that  $f_l = f_l(R_0, \Delta, u_0, \rho_0, S)$ , where  $u_0 = R_0\Omega_0$  is the disk velocity at  $R = R_0$ ,  $\rho_0$  is the air density and  $S$  is a shape parameter. In this paper, we ignore any effect that the variations of  $\Delta$  may have in  $f_l$ .

Denoting  $p_x = \dot{x}$  and  $p_y = \dot{y}$ , the Hamiltonian function associated with (2) is

$$H = \frac{1}{2}(p_x^2 + p_y^2) + \frac{1}{2}\omega^2(x^2 + y^2) + \frac{1}{4}\gamma(x^2 + y^2)^2 - Fx \cos(\Omega t) - Fy \sin(\Omega t), \quad (4)$$

with  $\Omega = n\Omega_0$ . The Hamiltonian (4) is that of a forced isotropic oscillator. Following Deprit [8], we carry out a canonical

transformation  $(x, y, p_x, p_y) \rightarrow (l, g, L, G)$  to Lissajous variables as

$$x = s \cos(g + l) - d \cos(g - l), \quad (5a)$$

$$y = s \sin(g + l) - d \sin(g - l), \quad (5b)$$

$$p_x = -\omega[s \sin(g + l) + d \sin(g - l)], \quad (5c)$$

$$p_y = \omega[s \cos(g + l) + d \cos(g - l)], \quad (5d)$$

with

$$s = \sqrt{\frac{L+G}{2\omega}}, \quad d = \sqrt{\frac{L-G}{2\omega}}, \quad L \geq 0, \quad |G| \leq |L|. \quad (6)$$

Here  $(l, g)$  are angle variables and  $(L, G)$  are their conjugate actions. The Hamiltonian becomes

$$H = \omega L - F[s \cos(g + l - \Omega t) - d \cos(g - l - \Omega t)] + \frac{\gamma}{4}[(s^2 + d^2) - 2sd \cos(2l)]^2. \quad (7)$$

For  $F = 0$ ,  $g$  becomes a cyclic variable, leaving its conjugate action,  $G = x\dot{y} - y\dot{x}$ , as an integral of motion. In such a circumstance, the time  $t$  does not appear in (7) explicitly, so  $H$  is the second integral of motion. We conclude that the system is completely integrable for  $F = 0$  and the phase space flows lie on the cross section of the two integral manifolds  $G$  and  $H$ . Closed form solutions of this integrable case have been given in Lakshmanan and Kaliappan [9] using Jacobi’s elliptic functions.

We carry out two successive canonical transformations  $(l, g, L, G) \rightarrow (Q_1, Q_2, P_1, P_2)$  and  $(Q_1, Q_2, P_1, P_2) \rightarrow (\theta_1, \theta_2, J_1, J_2)$  using the generating functions

$$S_2 = (g + l - \Omega t)P_1 + lP_2, \quad (8)$$

and

$$S_3 = -(P_1 + \frac{1}{2}P_2)\theta_1 - \frac{1}{2}P_2\theta_2, \quad (9)$$

respectively. These give

$$J_1 = \frac{1}{2}(L + G), \quad \theta_1 = g + l - \Omega t, \quad (10a)$$

$$J_2 = \frac{1}{2}(L - G), \quad \theta_2 = l - g + \Omega t, \quad (10b)$$

and the new Hamiltonian becomes  $\mathcal{H} = H + \partial S_2/\partial t$ . One can now express  $\mathcal{H}$  in terms of the new variables  $(\theta_1, \theta_2, J_1, J_2)$ . Defining  $\mu = \omega - \Omega$  we obtain

$$\mathcal{H} = (2\omega - \mu)J_2 + \mu J_1 - \frac{F}{\sqrt{\omega}}[\sqrt{J_1} \cos \theta_1 - \sqrt{J_2} \cos \theta_2] + \frac{\gamma}{4\omega^2}[(J_1 + J_2) - 2\sqrt{J_1 J_2} \cos(\theta_1 + \theta_2)]^2. \quad (11)$$

It is seen that  $\mathcal{H}$  does not explicitly depend on  $t$ . This is an interesting result because the dynamics is now reduced to a flow in the four-dimensional  $(\theta_1, \theta_2, J_1, J_2)$ -space with  $\mathcal{H} = h$  being an integral manifold. From (8) we obtain  $\mathcal{H} = H - \Omega G$ .

Noting that  $H$  is an energy function, the first integral  $\mathcal{H} = h$  is actually the total energy in a rotating frame of angular velocity  $\Omega$  in the  $(x, y)$ -space.

The equations of motion are obtained from  $\mathcal{H}$  as

$$\frac{d\theta_k}{dt} = \frac{\partial \mathcal{H}}{\partial J_k}, \quad \frac{dJ_k}{dt} = -\frac{\partial \mathcal{H}}{\partial \theta_k}, \quad k = 1, 2. \tag{12}$$

Since the orbits of (12) lie on the manifold  $\mathcal{H} - h = 0$ , one needs a second integral for solving the problem completely. Such an integral does not exist if some parts of the phase space are filled by chaotic orbits.

### 3. Poincaré maps

The phase space flows of (12) can be visualized using an appropriate surface of section  $\Sigma$  (Poincaré map). Let us define

$$\Sigma = \left\{ (J_1, J_2, \theta_1, \theta_2) \in \mathbb{R}^{2+} \times S^2 \mid \cos \theta_2 = 1 \right\}. \tag{13}$$

Since  $2\omega - \mu = \omega + \Omega$  is a positive and practically large number,  $\theta_2$  will be rotational for all flows. Therefore,  $\Sigma$  is a global section, which is transversally intersected by all flows. On this surface we have

$$\mathcal{H}(\theta_1, \theta_2 = 0, J_1, J_2) - h = 0. \tag{14}$$

System (12) is without escape and the admissible zone on  $\Sigma$ ,  $D_\Sigma$ , is obtained from (14) by imposing the requirement that both  $J_1$  and  $J_2$  are real positive.

Given  $h$ , we choose a pair  $\mathbf{P}_0 = [\theta_1(0), J_1(0)]$  on  $D_\Sigma$  and use it in (14) for computing  $J_2(0)$ . Together with  $\theta_2(0) = 0$ , these constitute a full set of initial conditions on  $D_\Sigma$ . We then numerically integrate Eqs. (12) and sample  $\mathbf{P} = (\theta_1, J_1)$  each time the orbit intersects  $\Sigma$ . This defines a map  $Q : D_\Sigma \rightarrow D_\Sigma$ , and one may write  $\mathbf{P}_{n+1} = Q(\mathbf{P}_n)$ , where  $\mathbf{P}_n$  is the  $n$ th image of  $\mathbf{P}_0$ . We take 1000 samples for each initial condition. Chaotic orbits need more samples (sometimes up to 2000) until they occupy their invariant measure. The most important information on  $D_\Sigma$  are the fixed points of  $Q$ , which correspond to periodic motions in  $\theta_2$ . Any  $m$ -cycle of  $Q$  is a  $2m\pi$ -periodic solution in  $\theta_2$ . The invariant tori around the fixed points of  $Q$  form resonant islands, which correspond to quasi-periodic orbits. Chaotic orbits can emerge in the vicinity of hyperbolic fixed points.

The global structure of the flows of (12) highly depends on the values of system parameters among which only  $\mu$  and  $F$  may vary in operational conditions (see Section 2).  $\mu$  varies during the acceleration and deceleration phases of the disk rotation. The parameters  $\omega$  and  $\gamma$  depend on  $U(R)$  and the geometry (inner and outer radii and thickness) and material of the disk. Therefore, they are constants. For simplicity, we set  $\omega = \gamma = 1$  and investigate how the variations in  $\mu$  and  $F$  influence the phase space flows. Our computations show that interesting cases happen for small values of  $|\mu|$  associated with motions in the vicinity of the 1:1 resonance. We find both integrable and non-integrable models whose topologies are explained below.

The first integrable form is obtained when a single resonant island occupies the phase space. Fig. 1 demonstrates the Poincaré map of this case for  $\mu = 0.2$ ,  $F = 0.2$  and  $h = 8$ . The

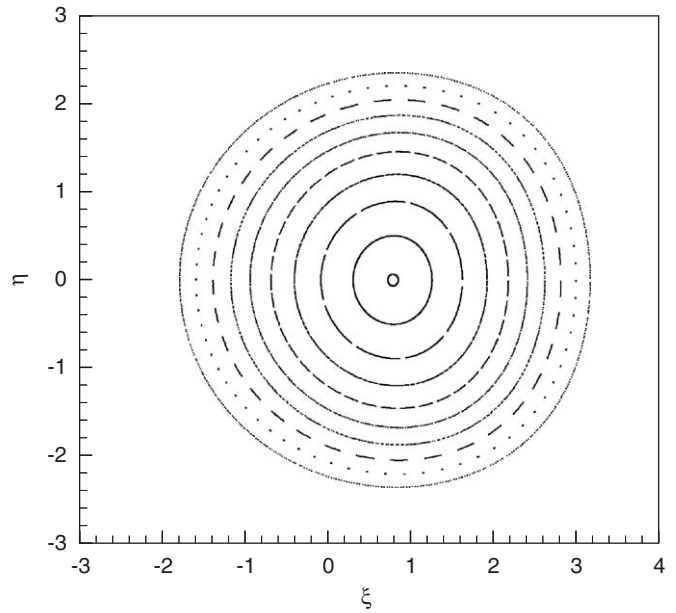


Fig. 1. Poincaré map for  $\mu = 0.2$ ,  $F = 0.2$  and  $h = 8$ . The phase space is occupied by the 1:1 resonant island. Here and below we have  $\xi = \sqrt{2J_1} \cos \theta_1$  and  $\eta = \sqrt{2J_1} \sin \theta_1$ .

only elliptic fixed point corresponds to a  $2\pi$ -periodic orbit in  $\theta_2$ . We have chosen  $\xi = \sqrt{2J_1} \cos \theta_1$  and  $\eta = \sqrt{2J_1} \sin \theta_1$  as the horizontal and vertical coordinates of our maps, respectively.

We now increase  $\mu$  and  $F$  while keeping  $h$  fixed. The second integrable form is observed for  $\mu = 0.8$  and  $F = 1$  in Fig. 2a. As this figure shows, the fundamental periodic orbit of Fig. 1 has been preserved, though it has moved a bit. A new elliptic 1-cycle has also appeared together with its resonant island. This island is confined to the homoclinic orbits of a hyperbolic fixed point. For a larger  $F$ , the system is non-integrable and chaotic orbits dominate the phase space (Fig. 2b). Nevertheless, many KAM tori do exist.

The third integrable geometry with a central 1-cycle and an elliptic 2-cycle is achieved for  $\mu = 0.2$ ,  $F = 1.5$  and  $h = 8$  (Fig. 2c). There are two hyperbolic fixed points (connected by two heteroclinic orbits) which correspond to an unstable periodic orbit of period  $4\pi$ . By increasing  $F$  to 4, a chaotic layer occurs near the hyperbolic fixed points through the destruction of heteroclinic orbits (Fig. 2d). The most interesting phenomenon observed in Fig. 2d is the occurrence of long-period cycles around the fundamental 2-cycle. The periods of these cycles increase outwards until they join the chaotic region.

Models with  $\mu < 0$  yet allow for new topologies. We have found the fourth and fifth integrable geometries with elliptic 3- and 4-cycle, respectively (Figs. 3a and c). Their resonant islands form a chain around the main central 1-cycle. Periodic  $m$ -cycles are destroyed and replaced by new generations of long-period resonant islands as  $F$  is increased. Fig. 3b shows a clear picture of this phenomenon. From the central 1-cycle outwards, we observe a sequence of 5-, 8-, 13- and 21-cycle which are indeed Fibonacci numbers. The outermost 8-cycle (seen as holes) has been immersed in the chaotic layer. It is possible

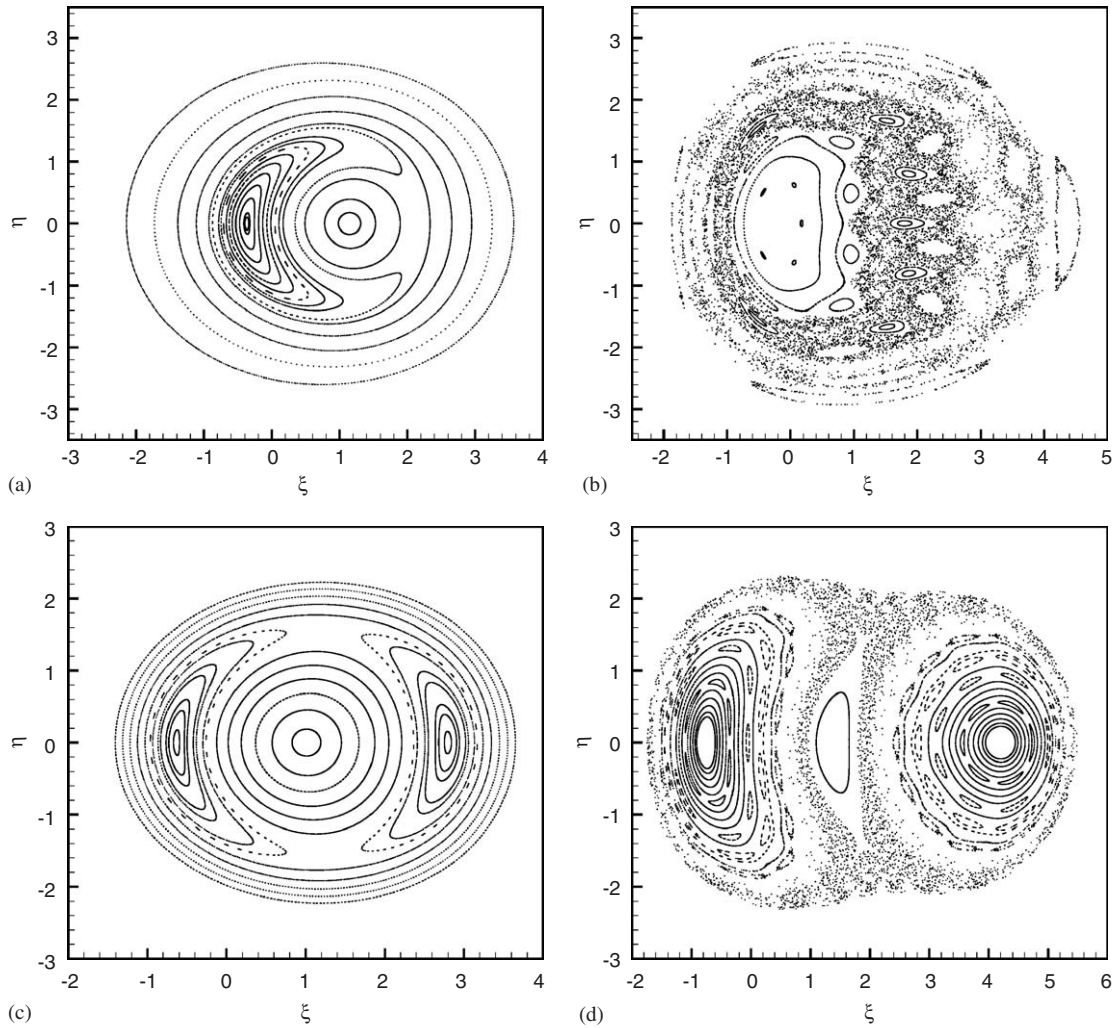


Fig. 2. Poincaré maps for  $\mu > 0$ : (a)  $\mu = 0.8$ ,  $F = 1$  and  $h = 8$ ; (b)  $\mu = 0.8$ ,  $F = 4$  and  $h = 8$ ; (c)  $\mu = 0.2$ ,  $F = 1.5$  and  $h = 8$ ; (d)  $\mu = 0.2$ ,  $F = 4$  and  $h = 8$ .

to increase  $F$  but still get a regular structure. Fig. 3d shows how the 4-cycle of its left panel is replaced by a powerful 7-cycle and a very weak (outer) 18-cycle while maintaining the regular nature of the flow. Our computations show that the first and second integrable geometries exist for  $\mu < 0$  as they do for  $\mu > 0$ . There is only a minor difference. For negative values of  $\mu$ , the topology of the second integrable form looks like the mirror image of Fig. 2a with respect to the  $\eta$ -axis.

Topologies shown in Figs. 2 and 3 are generic for two-dimensional area preserving maps. Our results are in harmony with the predictions made by Hénon [10] using an area preserving quadratic map. Hénon’s map has not yet been derived from a four-dimensional Hamiltonian vector field. According to Giovannozzi [11], however, it is possible to decompose area preserving, polynomial 2D diffeomorphisms to a sequence of quadratic Hénon maps. Therefore, a general 2D map is expected to inherit the properties of the Hénon map as our results show. Although the central 1:1 resonant island is present both in integrable and in non-integrable systems, only one or finite number of higher-order islands exist in integrable cases displayed in Figs. 2 and 3. The size of higher-order islands grows proportional to the strength of non-linearities, but it is then controlled

via the occurrence of outer islands. Our results clearly show this phenomenon. Similar results have also been pointed out and discussed by Contopoulos [12] for galactic systems.

#### 4. Adiabatic invariants in the presence of imperfections

So far, we have studied axisymmetric, initially flat disks. Imperfections and asymmetries, however, are likely in realistic systems. Raman and Mote [13] introduced a simple model for imperfect disks and derived the following equations for the amplitude functions:

$$\ddot{x} + \omega_c^2 x + \varepsilon \gamma (x^2 + y^2) x = \varepsilon F \cos(\Omega t), \tag{15a}$$

$$\ddot{y} + \omega_s^2 y + \varepsilon \gamma (x^2 + y^2) y = \varepsilon F \sin(\Omega t), \tag{15b}$$

with  $\varepsilon$  being a small perturbation parameter. For  $\varepsilon = 0$ , Eqs. (15) reduce to a system of anisotropic oscillators. Therefore, the transformation (5), which has been designed for elliptic oscillators (with  $\omega_s = \omega_c$ ), is no longer helpful. The particular  $F = 0$  case reminds us the equations of motion of stars inside elliptical galaxies investigated by Davoust [14] and Jalali et al. [15].

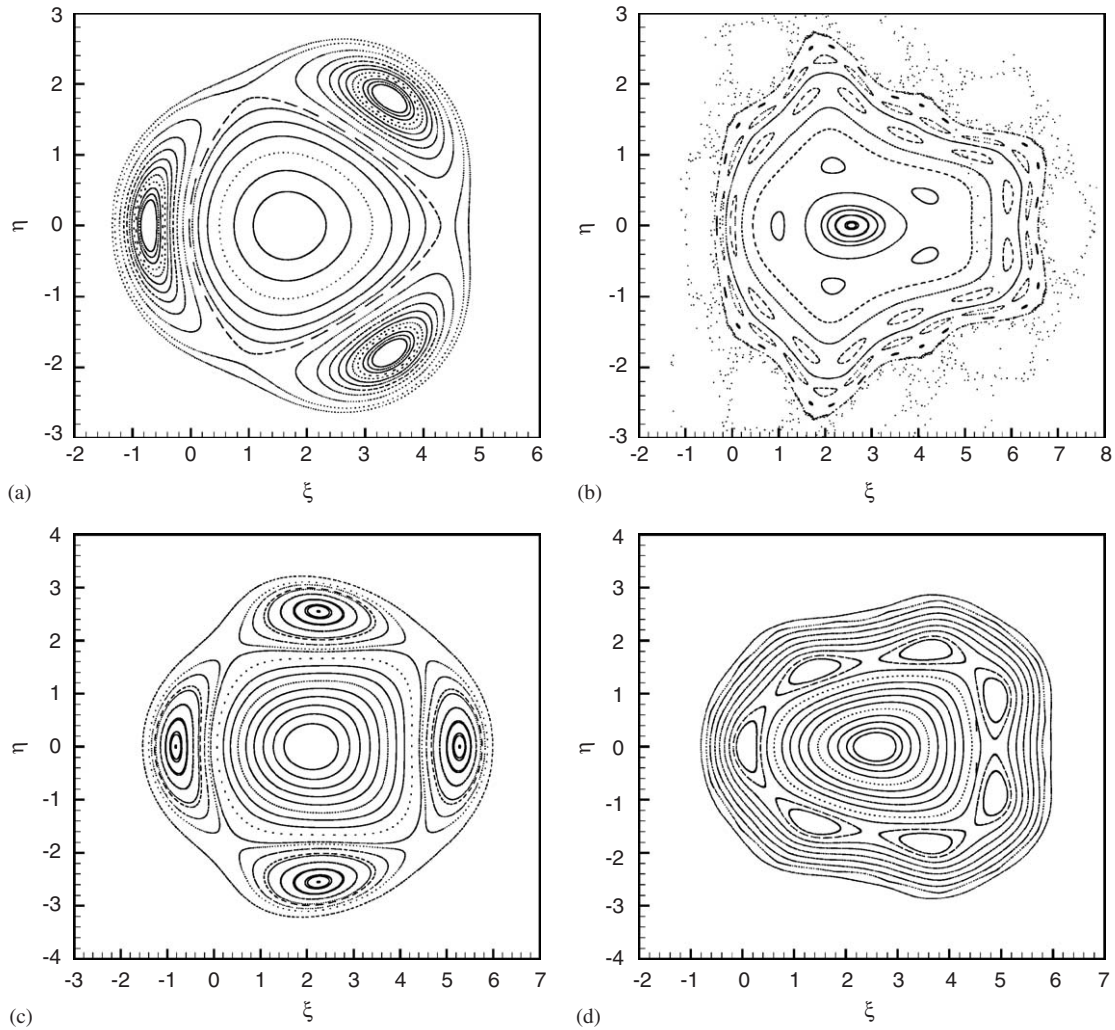


Fig. 3. Poincaré maps for  $\mu < 0$ : (a)  $\mu = -0.2$ ,  $F = 3$  and  $h = 10$ ; (b)  $\mu = -0.2$ ,  $F = 7$  and  $h = 10$ ; (c)  $\mu = -0.4$ ,  $F = 3$  and  $h = 8$ ; (d)  $\mu = -0.4$ ,  $F = 4.5$  and  $h = 8$ .

Periodic solutions of (15) for  $F = 0$  will be obtained using the results of Section 6 in [15] if we set  $W_{30} = W_{21} = W_{12} = W_{21} = \gamma$ ,  $W_{20} = \omega_c^2$  and  $W_{11} = \omega_s^2$ . Of course, the first (energy) integral does exist when  $F = 0$  and one can generate Poincaré maps to explore the phase space flows. For the general case with  $F \neq 0$ , however, we are not aware of any motion integral. The perturbation method based on infinitesimal Lie transforms is the only powerful analytical tool for exploring global phase space flows, but only when  $\omega_c^2/\omega_s^2 = m^2/n^2 + \varepsilon\eta$ . Here  $m$  and  $n$  are integers and  $\varepsilon\eta$  is an irrational real number with  $|\varepsilon\eta| \ll 1$ . In this paper we confine ourselves to the case  $m = n$ . The Hamiltonian function associated with (15) and in terms of Lissajous variables, reads

$$\begin{aligned}
 H = & \omega L - \varepsilon F [s \cos(g + l - \Omega t) - d \cos(g - l - \Omega t)] \\
 & + \varepsilon \frac{\gamma}{4} [(s^2 + d^2) - 2sd \cos(2l)]^2 \\
 & + \varepsilon \frac{\eta \omega^2}{4} [(s^2 + d^2) + s^2 \cos(2g + 2l) \\
 & + d^2 \cos(2g - 2l) - 2sd \cos(2g) - 2sd \cos(2l)]. \quad (16)
 \end{aligned}$$

Since  $\varepsilon$  is sufficiently small, the phase space topology associated with (16) is determined by  $\mu = \omega - \Omega$ . In the following subsections, we investigate the dynamics when  $\mu \ll 0$ ,  $\mu \gg 0$  and  $|\mu| \ll 1$ .

#### 4.1. High-speed disks: $\mu \ll 0$

When the angular velocity  $\Omega$  is very large compared to  $\omega$ ,  $\Omega t$  grows faster than  $l$  and the long-term behavior is determined by the first-order averaged Hamiltonian

$$\bar{H}_t = \langle H \rangle_t = \frac{\Omega}{2\pi} \int_{-\pi/\Omega}^{\pi/\Omega} H(\bar{l}, \bar{g}, \bar{L}, \bar{G}; t) dt.$$

The resulting equations of motion (for  $\bar{x}$  and  $\bar{y}$ ) will then take a form similar to (15) with  $F = 0$ . Here  $\bar{H}_t$  is an adiabatic invariant and one can generate Poincaré maps of the averaged system by sampling  $(\bar{x}, \bar{p}_x)$  when  $\bar{y} = 0$  and  $\bar{p}_y > 0$ . Periodic solutions of the averaged system, which also correspond to periodic orbits of (15), can easily be obtained using the method of [15] as we discussed earlier. Note that the effect of a

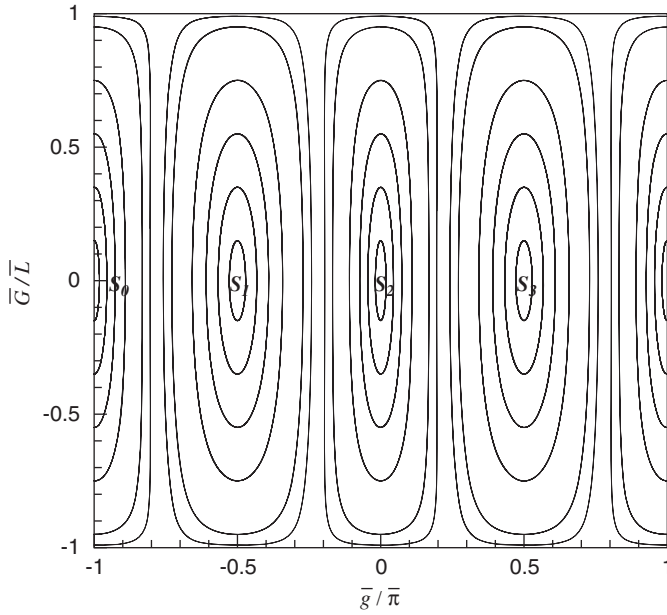


Fig. 4. Phase space flows of the normalized equations of motion obtained from  $\bar{H}_l$  for  $\eta\omega^3/\gamma=0.5$  and  $\bar{L}=0.2$ . All equilibrium points are centers.

high-frequency excitation (large  $\Omega$ ) does not occur up to first-order terms.

4.2. Low-speed disks:  $\mu \gg 0$

For  $\Omega \ll \omega$ ,  $\omega L$  becomes the dominant term in (16) and the first-order averaged Hamiltonian is defined as

$$\bar{H}_l = \langle H - \omega L \rangle_l = \frac{1}{2\pi} \int_{-\pi}^{\pi} [H(\bar{l}, \bar{g}, \bar{L}, \bar{G}; t) - \omega \bar{L}] d\bar{l}. \quad (17)$$

We obtain

$$\bar{H}_l = \varepsilon \frac{\gamma}{8\omega^2} (3\bar{L}^2 - \bar{G}^2) + \varepsilon \frac{\eta\omega}{4} \left[ \bar{L} - \sqrt{\bar{L}^2 - \bar{G}^2} \cos(2\bar{g}) \right], \quad (18)$$

which results in the following equations of motion

$$\begin{aligned} \bar{g}' &= \frac{\partial \bar{H}_l}{\partial \bar{G}} = -\frac{\gamma}{\eta\omega^3} \bar{G} + \bar{G} (\bar{L}^2 - \bar{G}^2)^{-1/2} \cos(2\bar{g}), \\ \bar{G}' &= -\frac{\partial \bar{H}_l}{\partial \bar{g}} = -2(\bar{L}^2 - \bar{G}^2)^{1/2} \sin(2\bar{g}). \end{aligned} \quad (19)$$

The prime ' denotes a derivative with respect to the slow time  $\tau = \varepsilon\eta\omega t/4$ .  $\bar{L}$  and the Hamiltonian  $\bar{H}_l$  are adiabatic invariants, so the averaged system is completely integrable. The type and location of stationary points of (19) determine the topology of phase space flows. Trivial stationary points are  $S_n \equiv (\bar{g}_n, \bar{G}_n) = (-\pi + n\pi/2, 0)$ . For  $\eta > 0$  and  $\bar{L} \leq \eta\omega^3/\gamma$  all stationary points are centers and  $\bar{g}(t)$  is always a librating phase as Fig. 4 shows. For  $\bar{L} \geq \eta\omega^3/\gamma$ , however, the stationary points  $S_{0,2}$  are saddles and  $S_{1,3}$  are centers. There are two other stationary points (both of center type) for  $\bar{L} \geq \eta\omega^3/\gamma$ . Their coordinates are given by

$$S_{4,5} \equiv (\bar{g}_{4,5}, \bar{G}_{4,5}) = \left( 0, \pm \left[ \bar{L}^2 - \eta^2 \omega^6 / \gamma^2 \right]^{1/2} \right). \quad (20)$$

A bifurcation of the phase space flows occurs when the invariant manifold terminating at the saddle points  $S_0$  and  $S_2$  switches from a heteroclinic to a homoclinic orbit. The implicit equation for this manifold is

$$\cos(2\bar{g}) = \left( \bar{L} - \frac{\gamma}{2\eta\omega^3} \bar{G}^2 \right) (\bar{L}^2 - \bar{G}^2)^{-1/2}. \quad (21)$$

For  $\gamma\bar{L} \geq 2\eta\omega^3$  Eq. (21) represents a heteroclinic orbit, which connects  $S_0$  to  $S_2$ . In the presence of heteroclinic orbits, the angle  $\bar{g}(\tau)$  can become rotational (always decreasing in time,  $\bar{g}' < 0$ ) as the left panel in Fig. 5 shows.  $\bar{g}(\tau)$  is librating inside the region enclosed with two intersecting heteroclinic orbits. For  $\gamma\bar{L} < 2\eta\omega^3$ ,  $\bar{g}(\tau)$  becomes oscillatory in the whole space, the heteroclinic orbit disappears and it is replaced by a homoclinic orbit (right panel in Fig. 5). We remark that the stationary points of the averaged equations correspond to  $2\pi$ -periodic orbits in  $l$ . Thus, the zeroth-order periodic solutions for  $x(t)$  and  $y(t)$  are obtained from (5) as

$$x(t) = A \cos(\omega t + \bar{g}_k) - B \cos(\bar{g}_k - \omega t), \quad (22a)$$

$$y(t) = A \sin(\omega t + \bar{g}_k) - B \sin(\bar{g}_k - \omega t), \quad (22b)$$

with  $k = 0, \dots, 5$ , and

$$A = \sqrt{\frac{\bar{L} + \bar{G}_k}{2\omega}}, \quad B = \sqrt{\frac{\bar{L} - \bar{G}_k}{2\omega}}. \quad (23)$$

Substituting from (22) into (1) leads to

$$\begin{aligned} \frac{w(R, \phi, t)}{U(R)} &= A \cos(n\phi - \omega t - \bar{g}_k) \\ &\quad - B \cos(n\phi + \omega t - \bar{g}_k). \end{aligned} \quad (24)$$

This is a circumferential wave, composed of a forward and a backward traveling wave of the same phase and angular velocity. For  $\eta = 0$  (without imperfection),  $\bar{G}$  becomes a motion constant and we obtain  $\bar{g} = -\gamma\bar{G}\tau/(4\omega^2) + \bar{g}(0)$ . For  $\eta < 0$  we have the same results of  $\eta > 0$  but with a phase shift of  $\pi/2$  in the  $\bar{g}$  variable:  $\bar{g}_{\eta < 0} = \bar{g}_{\eta > 0} + \pi/2$ .

4.3. Motion near the 1:1 resonance:  $|\mu| < 1$

Near the 1:1 resonance, when  $|\mu| = |\varepsilon\bar{\mu}|$  is small, we represent the Hamiltonian function (16) in the  $(\theta, \mathbf{J})$ -space using the canonical transformations (10). Therefore,  $(\omega + \Omega)J_2$  becomes the dominant term of the Hamiltonian with  $\theta_2$  and  $\Omega t$  being fast angles. The slow dynamics is then governed by

$$\begin{aligned} \bar{H}_1 &\equiv \langle H - (\omega + \Omega)J_2 \rangle_{\theta_2, t} \\ &= \frac{\Omega}{4\pi^2} \int_{-\pi}^{\pi} d\bar{\theta}_2 \int_{-\pi/\Omega}^{\pi/\Omega} dt \left[ H(\bar{\theta}, \bar{\mathbf{J}}; t) - (\omega + \Omega)J_2 \right]. \end{aligned} \quad (25)$$

It is seen that  $\bar{H}_1$  and  $\bar{J}_2$  are adiabatic invariants. We obtain

$$\begin{aligned} \bar{H}_1 &= \varepsilon\bar{\mu}J_1 - \varepsilon F \sqrt{\frac{\bar{J}_1}{\omega}} \cos \bar{\theta}_1 + \frac{\varepsilon\eta\omega}{4} (J_1 + J_2) \\ &\quad + \frac{\varepsilon\gamma}{4\omega^2} (J_1^2 + J_2^2 + 4J_1J_2). \end{aligned} \quad (26)$$

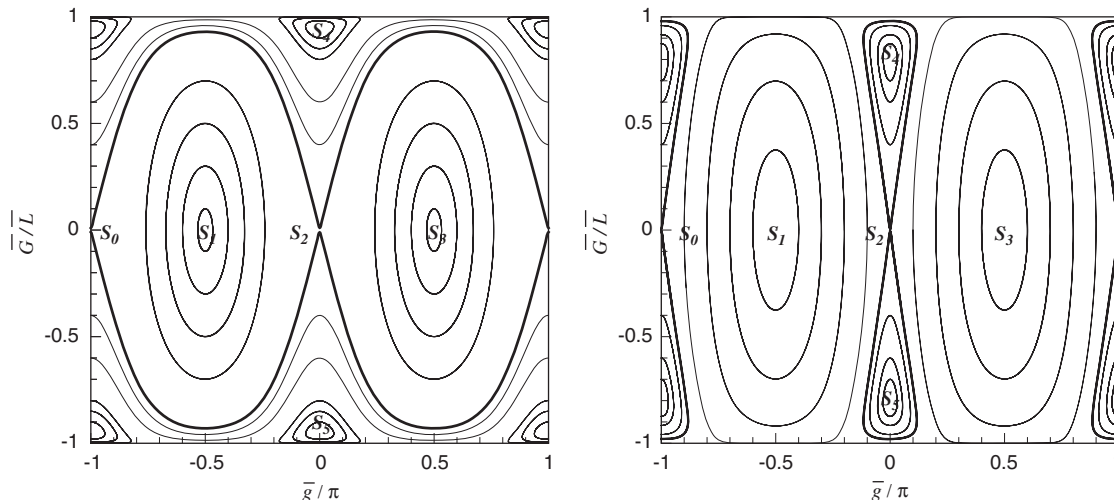


Fig. 5. Phase space flows of the normalized equations of motion obtained from  $\bar{H}_1$ . Left panel:  $\eta\omega^3/\gamma = \frac{3}{8}$  and  $\bar{L} = 1.2$ . The hyperbolic points  $S_0$  and  $S_2$  are connected by a heteroclinic orbit (thick line). Right panel:  $\eta\omega^3/\gamma = 1$  and  $\bar{L} = \frac{5}{3}$ . For  $\gamma\bar{L} < 2\eta\omega^3$ ,  $\bar{g}(t)$  can never be rotational and a homoclinic orbit (thick line) occurs around  $S_4$  ( $S_5$ ).

Denoting  $\hat{\mu} = \bar{\mu} + \eta\omega/4$ , equations of motion associated with (26) are obtained as

$$\frac{d\bar{\theta}_1}{dt} = \varepsilon \left( \hat{\mu} + \frac{\gamma\bar{J}_2}{\omega^2} \right) + \frac{\varepsilon\gamma\bar{J}_1}{2\omega^2} - \frac{\varepsilon F \cos \bar{\theta}_1}{2\sqrt{\omega\bar{J}_1}}, \tag{27a}$$

$$\frac{d\bar{J}_1}{dt} = -\varepsilon F \sqrt{\frac{\bar{J}_1}{\omega}} \sin \bar{\theta}_1. \tag{27b}$$

Equilibrium points of (27) are obtained by solving the cubic equation

$$u^3 + a_1u \pm a_0 = 0, \tag{28}$$

$$a_1 = 2\bar{J}_2 + \frac{2\hat{\mu}\omega^2}{\gamma}, \quad a_0 = \frac{\omega^{3/2}F}{\gamma},$$

for  $u = \sqrt{\bar{J}_1}$ . The plus and minus signs correspond to  $\bar{\theta}_1 = \pi$  and 0, respectively.  $\bar{J}_2$  is positive due to (6) and (10). Therefore, for  $\hat{\mu} > 0$  the discriminant of (28),  $D = a_1^3/27 + (27a_0/54)^2$ , is positive and the cubic equation has only one real solution. This solution corresponds to  $\bar{\theta}_1 = 0$ . In such a circumstance, the phase space is home for one resonant island similar to Fig. 1. For negative values of  $\hat{\mu}$ ,  $D$  can take non-positive values. For  $D = 0$ , a single solution exists for  $\bar{\theta}_1 = 0$  and a double solution for  $\bar{\theta}_1 = \pi$ . The single and double solutions correspond to a center and a cusp, respectively. For  $D < 0$ , the cubic equation has three real roots and we obtain two islands both at the 1:1 resonance. In such a circumstance, the global phase space geometry looks like the mirror image of Fig. 2a with respect to the vertical  $\eta$ -axis. The bifurcations of the phase portraits of (27) (due to variations in  $D$ ) belong to a well-known class illustrated in panels 1 through 2 of Fig. 71 in Arnold [16]. The stationary points of the averaged equations correspond to  $2\pi$ -periodic orbits in  $\theta_2$ . Denote  $(\theta_s, J_s)$  as the coordinates of a stationary point. The corresponding zeroth-order periodic

solutions for  $x(t)$  and  $y(t)$  are obtained from (5) as

$$x(t) = A \cos(\Omega t + \theta_s) - B \cos(\omega t + \beta), \tag{29a}$$

$$y(t) = A \sin(\Omega t + \theta_s) + B \sin(\omega t + \beta), \tag{29b}$$

with  $\beta = \theta_2(0)$ ,  $A = \sqrt{J_s/\omega}$  and  $B = \sqrt{\bar{J}_2/\omega}$ . Substituting from (29) into (1) leads to

$$\frac{w(R, \phi, t)}{U(R)} = A \cos(n\phi - \Omega t - \theta_s) - B \cos(n\phi + \omega t + \beta). \tag{30}$$

This *circumferential* wave is composed of a forward and a backward traveling wave of different frequencies and phase angles. They, respectively, correspond to the first and the second terms on the right-hand side of (30). For quasi-periodic orbits,  $\bar{J}_1$  and  $\bar{\theta}_1$  vary in  $\tau$  (according to (27)) and the amplitude and phase angle of the forward traveling wave become *slowly varying* functions of time.

### 5. Damping effect

The formulation adopted in this paper allows us to investigate the effect of structural damping in a straightforward fashion. The structural damping is entered to the equations of motion by adding the damping forces  $-2c p_x$  and  $-2c p_y$  to the right-hand sides of equations (2a) and (2b), respectively [2,3]. Here  $c > 0$  is the damping coefficient. The virtual work done by non-conservative damping forces is therefore obtained as

$$\delta W = -2c(p_x \delta x + p_y \delta y), \tag{31}$$

with  $\delta$  being the usual variation symbol. Substituting from (5) in (31) gives

$$\delta W = F_l \delta l + F_g \delta g + F_L \delta L + F_G \delta G, \tag{32a}$$

$$= F_1^0 \delta \theta_1 + F_2^0 \delta \theta_2 + F_1^J \delta J_1 + F_2^J \delta J_2, \tag{32b}$$

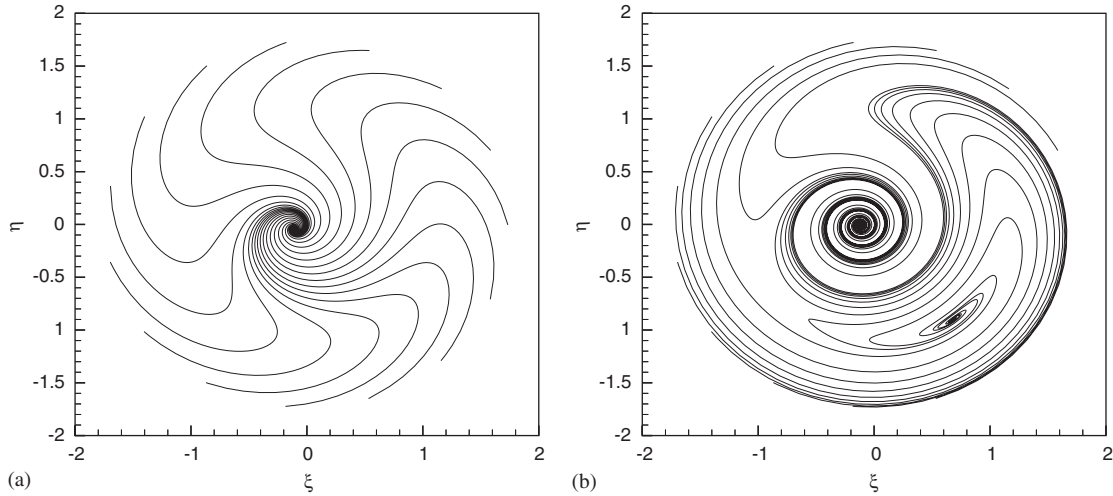


Fig. 6. Phase space flows of the normalized equations of a damped model with  $\hat{\mu} = -0.6$ ,  $\omega = 1$ ,  $\gamma = 2$  and  $F = 0.1$ . The coordinates are  $\xi = \sqrt{2J_1} \cos \bar{\theta}_1$  and  $\eta = \sqrt{2J_1} \sin \bar{\theta}_1$ : (a)  $c = 0.2$ , (b)  $c = 0.05$ .

with

$$F_k^\theta = -2c \left[ J_k + \sqrt{J_1 J_2} \cos(\theta_1 + \theta_2) \right], \quad (33a)$$

$$F_k^J = -c \frac{1}{J_k} \sqrt{J_1 J_2} \sin(\theta_1 + \theta_2), \quad k = 1, 2, \quad (33b)$$

$$F_l = -2c \left[ L + \sqrt{L^2 - G^2} \cos(2l) \right], \quad (33c)$$

$$F_g = -2cG, \quad (33d)$$

$$F_L = \frac{-cL}{\sqrt{L^2 - G^2}} \sin(2l), \quad (33e)$$

$$F_G = \frac{cG}{\sqrt{L^2 - G^2}} \sin(2l). \quad (33f)$$

Denoting  $\mathcal{L} = L\dot{l} + G\dot{g} - \mathcal{H}$  as the Lagrangian associated with  $\mathcal{H}$  (this is the well-known Legendre transformation), Hamilton's principle for non-conservative systems

$$\int_{t_1}^{t_2} (\delta \mathcal{L} + \delta W) dt = 0, \quad (34)$$

results in the following set of ODEs for the evolution of Lisajous variables

$$\frac{du}{dt} = \frac{\partial \mathcal{H}}{\partial v} - F_v, \quad \frac{dv}{dt} = -\frac{\partial \mathcal{H}}{\partial u} + F_u, \quad (35)$$

where  $u = (l, g)$  and  $v = (L, G)$ . The resonant  $(\theta, \mathbf{J})$  variables will also evolve according to

$$\frac{d\theta_k}{dt} = \frac{\partial \mathcal{H}}{\partial J_k} - F_k^J, \quad \frac{dJ_k}{dt} = -\frac{\partial \mathcal{H}}{\partial \theta_k} + F_k^\theta, \quad k = 1, 2. \quad (36)$$

Eqs. (35) and (36) do not admit any integral of motion.  $\mathcal{H}$  is no longer a constant along orbits, and therefore, the surface of section introduced in Section 3 cannot be used for visualizing the flows of (35) and (36). All invariant tori are destroyed for

$c \neq 0$  and quasi-periodic orbits no longer exist. Hyperbolic fixed points are preserved for sufficiently small values of  $c$  but elliptic points become spiral sinks (limit sets) and attract some flows. We demonstrate this scenario using reduced equations of motion when  $c$  is sufficiently small,  $c = \varepsilon \bar{c} = \mathcal{O}(\varepsilon)$ . When  $\omega \gg \Omega$ , we carry out a near-identity transformation  $(l, g, L, G) \rightarrow (\bar{l}, \bar{g}, \bar{L}, \bar{G})$  using Kamel's [17,18] method and average Eqs. (35) over the fast angle  $l$  up to the first-order terms in  $\varepsilon$ . This leads to the normalized equations

$$\frac{d\bar{g}}{d\tau} = -\frac{\gamma}{4\omega^2} \bar{G} + \frac{\eta\omega}{4} \bar{G} (\bar{L}^2 - \bar{G}^2)^{-1/2} \cos(2\bar{g}), \quad (37a)$$

$$\frac{d\bar{G}}{d\tau} = -\frac{\eta\omega}{2} (\bar{L}^2 - \bar{G}^2)^{1/2} \sin(2\bar{g}) - 2\bar{c}\bar{G}, \quad (37b)$$

$$\frac{d\bar{L}}{d\tau} = -2\bar{c}\bar{L}, \quad \tau = \varepsilon t. \quad (37c)$$

$\bar{L}$  tends to zero according to (37c). Simultaneously,  $\bar{G}$  and  $\bar{g}$  must tend to zero due to (37) and the natural constraint  $|\bar{G}| \leq \bar{L}$ . Hence, the warped rotating disk recovers its flat state in the presence of structural damping. The time scale of this flattening is of  $\mathcal{O}(1/\varepsilon)$ . Following a similar procedure near the 1:1 resonance, we obtain the following equations in the space of resonant variables:

$$\frac{d\bar{\theta}_1}{d\tau} = \left( \hat{\mu} + \frac{\gamma \bar{J}_2}{\omega^2} \right) + \frac{\gamma \bar{J}_1}{2\omega^2} - \frac{F \cos \bar{\theta}_1}{2\sqrt{\omega \bar{J}_1}}, \quad (38a)$$

$$\frac{d\bar{J}_1}{d\tau} = -F \sqrt{\frac{\bar{J}_1}{\omega}} \sin \bar{\theta}_1 - 2\bar{c}\bar{J}_1, \quad (38b)$$

$$\frac{d\bar{J}_2}{d\tau} = -2\bar{c}\bar{J}_2, \quad \tau = \varepsilon t, \quad (38c)$$

which are reduced to Eqs. (27) when  $\bar{c}=0$ . An immediate result is obtained by solving (38c). It gives  $\bar{J}_2(t) = \bar{J}_2(0)e^{-2\bar{c}t}$ . So  $\bar{J}_2(t)$  vanishes as  $t \rightarrow \infty$  and we may set  $\bar{J}_2 = 0$  in (38a). We

can now display possible phase space flows of (38). Stationary points of (38), with the coordinates  $(\theta_s, J_s)$ , satisfy  $\sin \theta_s = -2\bar{c}\sqrt{\omega J_s}/F$  from which one can compute  $\cos \theta_s$  and insert the result in (38a) to obtain

$$J_s^3 + \frac{4\hat{\mu}\omega^2}{\gamma} J_s^2 + \frac{4(\hat{\mu}^2 + \bar{c}^2)\omega^4}{\gamma^2} J_s - \frac{F^2\omega^3}{\gamma^2} = 0. \quad (39)$$

This cubic equation has only one real solution if  $\bar{c}^2 > \hat{\mu}^2/3$ . It corresponds to an attracting stationary point as shown in Fig. 6a. Eq. (39) has three real positive solutions if

$$\left(\frac{1}{3}\bar{c}^2 - \frac{1}{9}\hat{\mu}^2\right)^3 + \left(\frac{8\hat{\mu}\bar{c}^2}{3\gamma^3} + \frac{F^2}{2\omega^3\gamma^2} + \frac{8\hat{\mu}^3}{27\gamma^3}\right)^2 < 0. \quad (40)$$

Eqs. (38) will have one hyperbolic equilibrium point and two attracting foci if inequality (40) holds. The hyperbolic point corresponds to an unstable limit cycle and the attracting foci correspond to stable ones (Fig. 6b). The stable cycle with the largest amplitude should be avoided in practice. One possible way is to guide the state of the system to the basin of attraction of the cycle with the smallest amplitude. Given  $\bar{J}_2 = 0$  for a dissipative system, Eq. (30) implies

$$w(R, \phi, t) = A \cdot U(R) \cos(n\phi - \Omega t - \theta_s), \quad (41)$$

which is a forward traveling circumferential wave. A large structural damping that violates (40), results in an almost flat state of the spinning disk, i.e.,  $A \approx 0$  and  $w \approx 0$ .

## 6. Conclusions

In this paper, we adopted a Hamiltonian formulation for studying the dynamics of a forced isotropic oscillator, which arises in transversal vibration analysis of rotating disks. Applications of our findings are mainly in computer industry. The fundamental achievement of this paper was to reveal the existence of the first (non-trivial) integral of motion using two successive canonical transformations. Our first integral (for  $F \neq 0$ ) has not already been reported in the literature. The existence of the new integral manifold allowed us to make a global exploration of phase space flows. In Section 4, we generated adiabatic invariants when the terms involving  $\mu$ ,  $\eta$ ,  $\gamma$  and  $F$  were small. For  $\eta \neq 0$ , we found a new kind of bifurcations in the orbital structure: switching from a heteroclinic to a homoclinic orbit. Our reduced equations of motion in the presence of damping effects, and their corresponding approximate solutions, are also new. Without our Hamiltonian formalism, it was a cumbersome task to predict and visualize the phase space topology of the damped system.

Sections 2 and 3 of this paper were dedicated to the global behavior of perfect rotating disks ( $\eta = 0$ ). For such systems search in the parameter space shows that the orbital structure is highly sensitive to  $\mu = \omega - \Omega$ . Far from resonances and for large and positive values of  $\mu$ , we arrive at a topology similar to that of Fig. 1. Our further numerical experiments show that the fundamental periodic orbit departs from the center as  $|\mu|$  is increased. Taking the dissipation effect into account, this means

that the amplitude of the attracting limit cycle (e.g., Fig. 6a) increases proportional to  $|\mu|$ . In the presence of damping, the state of the system is guided towards one of the stable limit cycles that emerge from the central periodic orbits of resonant islands. The innermost limit cycle has usually the smallest amplitude, and therefore, it is the best candidate for nominal operation of a high-speed rotating disk near the 1:1 resonance. Our results for  $c = 0$  show that  $w(R, \phi, t)$  is composed of a forward and a backward traveling wave. Damped system, however, supports only the forward traveling wave as  $t \rightarrow \infty$ .

Once  $\mu$  is fixed,  $F$  will be the only variable that controls the nature of orbits. Integrable forms, and consequently regular orbits, do exist when  $F$  is small. We must avoid chaotic and higher-order resonant orbits that give rise to large-amplitude oscillations. They occur for large values of  $F$ . According to (3), a practical way to suppress chaotic vibrations of a HDD is to control the magnitude of  $F$  via changing  $R_0$  temporarily. This needs a *slow* maneuver of the head in the radial direction. It is remarked that Eqs. (2) have been obtained by assuming that  $f_i$  has a fixed radial position at  $R = R_0$ . Our results are still reliable if  $R_0$  is changed in a time scale longer than the rotational period of the disk.

Nowinski's [1] governing equations are obtained by assuming that the in-plane inertias  $(u, v)\Omega^2$ ,  $2\Omega(u_{,t}, v_{,t})$  and  $(u_{,tt}, v_{,tt})$  are small against  $r\Omega^2$  ( $r_i < r < r_o$ ). The rotary inertia  $r\Omega^2$  is then distributed between the in-plane stress components  $N_{rr}$ ,  $N_{\theta\theta}$  and  $N_{r\theta}$ . This assumption does not imply that in-plane modes cannot be excited by lateral vibrations, as they really do. This is perhaps the major drawback of Nowinski's theory. In their recent formulation of the spinning disk problem, Baddour and Zu [19] derived the most complete set of governing equations that involve all in-plane and lateral effects, including inertias quoted above. They discussed that the ignorance of in-plane inertias is not justified for rotating disks although it is a first-order approximation for non-rotating ones. The second part of their work [20] was dedicated to finding linear transverse modes. Search for global non-linear solutions of Baddour and Zu's [19] model, however, remains as a challenging problem, for a stress function no longer exists in the presence of in-plane inertias. Also, closed-form expressions are still unavailable for eigenfunctions that may be used to expand physical quantities in spatial coordinates.

## Acknowledgments

We wish to thank the referees for their enlightening comments that helped us to improve the results and presentation of this work. M. A. J. thanks the Research Vice-Presidency at Sharif University of Technology for partial support.

## References

- [1] J. Nowinski, Nonlinear transverse vibrations of a spinning disk, ASME J. Appl. Mech. (1964) 72.
- [2] A. Raman, C.D. Mote Jr., Nonlinear oscillations of circular plates near a critical speed resonance, Int. J. Non-Linear Mech. 34 (1999) 139.

- [3] A. Raman, C.D. Mote Jr., Remarks on the nonlinear vibration of an axisymmetric circular disk near critical speed, *Int. J. Non-Linear Mech.* 37 (2002) 35.
- [4] J.N. Reddy, *Applied Functional Analysis and Variational Methods in Engineering*, McGraw-Hill, New York, 1986.
- [5] A.C.J. Luo, C.A. Tan, Resonant and stationary waves in rotating disks, *Nonlinear Dyn.* 24 (2001) 359.
- [6] D. Lee, A.M. Waas, B.H. Karnopp, Analysis of a rotating multi-layer annular plate modeled via layer-wise zig zag theory: free vibration and transient analysis, *Comput. Struct.* 66 (1998) 313.
- [7] D. Lee, A.M. Waas, Stability analysis of a rotating multi-layer annular plate with a stationary frictional follower load, *Int. J. Mech. Sci.* 39 (1997) 1117.
- [8] A. Deprit, The Lissajous transformation. I—Basics, *Celest. Mech. Dyn. Astron.* 51 (1991) 201.
- [9] M. Lakshmanan, P. Kaliappan, On the energy levels of an isotropic anharmonic oscillator, *J. Phys. A* 13 (1980) L299.
- [10] M. Hénon, Numerical study of quadratic area-preserving mappings, *Quart. Appl. Math.* 27 (1969) 291.
- [11] M. Giovannozzi, Stability domain and invariant manifolds of 2d area-preserving diffeomorphisms, *Celest. Mech. Dyn. Astron.* 68 (1997) 177.
- [12] G. Contopoulos, *Order and Chaos in Dynamical Astronomy*, Springer, New York, 2002.
- [13] A. Raman, C.D. Mote Jr., Effects of imperfection on the non-linear oscillations of circular plates spinning near critical speed, *Int. J. Non-Linear Mech.* 36 (2001) 261.
- [14] E. Davoust, Periodic orbits in elliptical galaxies, *Astron. Astrophys.* 125 (1983) 101.
- [15] M.A. Jalali, B. Mehri, S.H. Pourtakdoust, Investigation of periodic orbits in elliptical galaxies using the method of implicit functions, *Celest. Mech. Dyn. Astron.* 63 (1996) 271.
- [16] V.I. Arnold, *Mathematical Aspects of Classical and Celestial Mechanics*, Springer, New York, 1993.
- [17] A.A. Kamel, Expansion formulae in canonical transformations depending on a small parameter, *Celest. Mech.* 1 (1969) 190.
- [18] A.A. Kamel, Perturbation method in the theory of nonlinear oscillations, *Celest. Mech.* 3 (1970) 90.
- [19] N. Baddour, J.W. Zu, A revisit of spinning disk models, Part I: derivation of equations of motion, *Appl. Math. Modeling* 25 (2001) 541.
- [20] N. Baddour, J.W. Zu, A revisit of spinning disk models, Part II: linear transverse vibrations, *Appl. Math. Modeling* 25 (2001) 561.